Formation of Kr^{3+} via core-valence doubly ionized intermediate states

E. Andersson,[1] P. Linusson,[2] S. Fritzsche,[3,4,5] L. Hedin,[1] J. H. D. Eland,[1,6] L. Karlsson,[1] J.-E. Rubensson,[1] and R. Feifel[1]

[1]*Department of Physics and Astronomy, Uppsala University, Box 516, SE-751 20 Uppsala, Sweden*

[2]*Department of Physics, Stockholm University, AlbaNova University Centre, SE-106 91 Stockholm, Sweden*

[3]*Department of Physics, P. O. Box 3000, Fin-90014 University of Oulu, Finland*

[4]*GSI Helmholtzzentrum für Schwerionenforschung D-64291 Darmstadt, Germany*

[5]*Frankfurt Institute for Advanced Studies, D-60438 Frankfurt am Main, Germany*

[6]*Department of Chemistry, Physical and Theoretical Chemistry Laboratory, Oxford University, South Parks Road, Oxford OX1 3QZ, United Kingdom*

(Received 22 December 2011; published 5 March 2012)

The time-of-flight photoelectron-photoion coincidence technique has been used to study single-photon $3d^9 4p^5$ core-valence double ionization of Kr and subsequent Auger decay to triply charged states associated with the $4s^2 4p^3$ and $4s^1 4p^4$ configurations. The photon energy used was $h\nu = 150$ eV. Multiconfiguration Dirac-Fock calculations were performed both for the doubly ionized intermediate states and the triply ionized final states. The intermediate states of Kr^{2+} are observed between 120 and 125 eV, whereas the final states of Kr^{3+} are observed between 74- and 120-eV ionization energy. Assignments of all structures are made based on the present numerical results. The calculated Auger rates give a detailed explanation of the relative line strengths observed.

DOI: 10.1103/PhysRevA.85.032502 PACS number(s): 33.70.Ca, 33.80.Eh, 34.50.Gb

I. INTRODUCTION

Conventional photoelectron spectroscopy (see, e.g., Refs. [1–3]) is known to give important information on the electronic structure of mainly singly ionized species. To study the electronic states of doubly and more highly charged systems, Auger-electron spectroscopy (see, e.g., Refs. [1,3]) has been used for many years. In order to fully characterize multi-ionization processes, coincidence experiments, which involve simultaneous detection of several species born together in a single event, are of great advantage. Recently, a versatile multielectron coincidence spectroscopy technique based on a magnetic bottle [4] has been presented by Eland *et al.* [5] which allows for the analysis of the kinetic energy of several electrons originating from the same ionization event.

The formation of triply charged electronic states on single-photon absorption can occur in several different ways. The three electrons can be emitted either directly or indirectly as recently investigated for valence shell ionization in the works of Hikosaka *et al.* [6] and Eland *et al.* [7]. If an inner shell is involved, the following two indirect processes can be distinguished: (a) single inner-shell ionization with subsequent double Auger decay and (b) core-valence double ionization with additional single Auger decay. Double Auger decay has recently been investigated by Penent *et al.* [8] and Viefhaus *et al.* [9] for initial Xe $4d$, by Lablanquie *et al.* [10] for initial Ar $2p$, and by several groups [9,11–13] for initial Kr $3d$ ionization. The triple ionization pathway through core-valence doubly ionized intermediate states is less explored.

In the present work, we investigate both experimentally and theoretically the formation of Kr^{3+} states via core-valence intermediate states with a vacancy in the $3d$ inner shell. The population of several tricationic states of Kr is studied experimentally for selected $3d^{-1}\ 4p^{-1}$ doubly ionized states and compared to the results of multiconfiguration Dirac-Fock (MCDF) calculations.

II. EXPERIMENTAL DETAILS

The experiments were performed at beamline U49/2 PGM-2 [14] at the BESSY-II storage ring in Berlin, using essentially the same setup as has previously been described (see, e.g., Ref. [15] and references therein). Briefly, multielectron coincidences were detected using a ∼2-m-long magnetic bottle time-of-flight spectrometer [5,7] capable of resolving individual electron kinetic energies. The resolving power of the apparatus for single electrons can be expressed as a fixed numerical resolution $E/\Delta E$ of about 50 for electron energies above 1 eV and a fixed resolution ΔE of about 20 meV at lower energies. Commercially obtained Kr gas of a stated purity of >99.99% was let into the interaction region of the spectrometer through a hypodermic needle and then ionized by 150-eV photons. The Kr triple ionization data presented here were gathered during approximately 45 min. The electron flight times were referenced to the synchrotron light pulses, which have a width of about 30 ps and a periodicity of ∼800.5 ns [16] in single-bunch operation of the BESSY-II storage ring. In order to avoid accidental coincidences, the electron count rates were restricted to 3000/s, which resulted in an average three-electron coincidence rate of 66/s. This was achieved by closing the exit slit of the monochromator, whereby the intensity of the synchrotron light was suitably reduced. As a consequence, the energy resolution of the light was not a limiting factor for the measurements. The photon energy was calibrated using literature values of the Kr $3d$ near edge x-ray absorption spectrum [17] while the time to energy conversion was calibrated using known energies of Xe and Kr Auger lines [18].

III. THEORY AND COMPUTATIONS

A. Double-photoionization amplitudes

While atomic photoionization of single electrons has been studied for many decades, little is known about the simultaneous ionization of two electrons in a weak photon field.

This process needs at least second-order perturbation theory for its description and requires, apart from the electron-photon coupling, at least an additional electron-electron interaction to mediate the process. In a simplified model, some *shake-off* probabilities can be estimated from the overlap of the one-electron orbitals of the initial and final bound state, but this model assumes that the major part of the excess energy of the photoionization is carried away by one of the electrons. No detailed theoretical studies are known so far for many-electron atoms where the two-electron continuum has been treated explicitly.

For describing the double photoionization of atoms and ions, electric-dipole amplitudes are needed

$$D(\omega;\, \gamma_f J_f P_f, \epsilon_1\kappa_1, \epsilon_2\kappa_2 : \gamma_t J_t P_t) \tag{1}$$

which connects the initial state $|\psi_i\rangle \equiv |\psi(\gamma_i J_i P_i)\rangle$ with some allowed final state $|\psi(\gamma_f J_f P_f)\rangle$ of the photoion and the two photoelectrons in the continuum. In this notation of the double photo ionization (amplitudes), the atomic bound states $|\psi(\gamma J P)\rangle$ have a well-defined total energy E as well as total angular momentum J and parity P, while γ is used to denote all further quantum numbers that are needed to specify the state uniquely. Moreover, we here assume the photoelectrons to escape by means of the partial waves $|\epsilon_1\kappa_1\rangle$ and $|\epsilon_2\kappa_2\rangle$ and with the kinetic energies ϵ_1 and ϵ_2, respectively. Only the sum of these two energies $\epsilon_1 + \epsilon_2 = E_i + \omega - E_f$ is determined by the photon energy ω and the total energies of the ion in the initial and final states, respectively. The "photoion + two electrons" system then gives rise to the total final state $|\psi_t\rangle \equiv |\gamma_f J_f P_f, \epsilon_1\kappa_1, \epsilon_2\kappa_2 : \gamma_t J_t P_t\rangle$ with the total energy $E_t = E_i + \omega$, after the photon has been absorbed by the atom. As appropriate for a relativistic description of the bound-state electron density and the outgoing photoelectron, here we make use of the relativistic angular-momentum quantum number

$$\kappa = \pm(j + 1/2) \quad \text{for} \quad l = j \pm 1/2$$

in order to denote the symmetry properties of the outgoing electron, i.e., its angular momentum j *and* parity $(-1)^l$ [19].

Indeed, the dipole amplitudes [Eq. (1)] are the *building* blocks for calculating the cross sections and relative intensities in the double photoionization of atoms and ions [20]; from these amplitudes the cross section (intensity) for the simultaneous emission of two electrons

$$\sigma = \frac{4\pi^2\,\alpha\,\omega}{3(2J_i+1)} \sum_{\kappa_1, J_t} |D(\omega;\, \gamma_f J_f P_f, \epsilon_1\kappa_1, \epsilon_2\kappa_2 : \gamma_t J_t P_t)|^2 \tag{2}$$

is obtained by taking the sum over all the possible scattering states of the photoion in the final state $|\psi(\gamma_f J_f P_f)\rangle$ and with total energy $E_t = E_i + \hbar\omega$. Obviously, this includes the summation over the partial waves of each of the photoelectrons as well as over all final states $|\psi(\gamma_t J_t P_t)\rangle$ in the two-electron continuum with total angular momentum J_t and parity P_t. Apart from the intensities, the same dipole amplitudes also determine the angular distribution of the electrons as well as the alignment and orientation of the photoion and, thus, affect the subsequent photon or electron emission as far as this is allowed energetically [21].

Unfortunately, the computation of the dipole amplitudes [Eq. (1)] is hampered by the fact that the initial and final ionic states have a quite different electronic structure which cannot be connected formally by any one-electron operator as, for instance, the coupling of the electrons to the photon field. To avoid the summation over a complete spectrum of the many-electron system (in second- or higher-order perturbation theory), one needs to account at least for the relaxation of the electron density due to the emission of the two electrons. This relaxation of the density is seen most easily from the one-electron orbital functions in the wave function of the initial and final ionic states, which are not quite orthogonal to each other. To understand the computation of the dipole amplitudes [Eq. (1)] in more detail, we shall, first, explain how the atomic states were generated and utilized in the evaluation of these many-electron amplitudes.

B. Generation of wave functions

To compute the amplitudes [Eq. (1)], at least the final ionic states $|\psi(\gamma_f J_f P_f)\rangle$ typically refer to highly correlated (many-electron) states that are embedded energetically in the continuum of the photoion. To describe the wave functions of free atoms (and ions), the MCDF method has been found a versatile tool for the computation of energies and transition amplitudes, and especially if inner-shell electrons or several open shells are involved in the computations [19,22]. In this method, an atomic state is approximated by a linear combination of configuration state functions (CSF) of the same symmetry

$$\psi_\alpha(PJ) = \sum_{r=1}^{n_c} c_r(\alpha)\, |\gamma_r PJ\rangle, \tag{3}$$

where n_c is the number of CSF and $\{c_r(\alpha)\}$ denotes the representation of the atomic state in this many–electron basis. In most standard computations, the CSF are constructed as antisymmetrized products of a common set of orthonormal orbitals and are optimized on the basis of the Dirac-Coulomb Hamiltonian. Further contributions to the representation $\{c_r(\alpha)\}$ of the atomic states due to the relativistic Breit interaction have been added, while all other corrections are typically small for a medium-Z element such as krypton.

Applying the ansatz [Eq. (3)] for the ground and the $3d^9\,4p^5$ double hole states of krypton, the transition amplitudes [Eq. (1)] are traced back to the computation of the corresponding interaction matrix within the given CSF basis. To this end, the wave functions from the well-known GRASP92 code [23] have been utilized within the RATIP program [24] in order to evaluate all dipole amplitudes as indicated above. Both codes allow the inclusion of the dominant effects from relativity and correlations within the same computational framework.

C. Double-photoionization cross sections and relative intensities

The interaction of atoms with light leads to electron emission if the energy of the incident photon exceeds the ionization threshold. For wavelengths $\lambda_{\rm ph} \gg r_{\rm atom}$, i.e., if the electric-dipole ($E1$) approximation is appropriate, the absorbed photon always transfers an angular momentum

$L = 1$ and results in a change in the parity of the overall system "photoion + two electrons." In most cases, however, the photoion will be left in a final *hole* state where just one of the electrons is removed from the (electronic) configuration of the initial state $|\psi_i\rangle$, while the formation of double hole states is less likely. A simultaneous ionization of two or more electrons requires a *correlated* motion of the electrons, and its photoionization amplitude becomes nonzero only in second-order perturbation theory (i.e., if the electron-electron interaction is applied to contribute to an additional order in the perturbation expansion).

To, at least, estimate the size of these second-order amplitudes, we made use of the relaxation of the bound-state density by performing an independent optimization for the initial and final ionic states. Such a computational procedure leads to orbital functions for the initial and final states that are no longer orthogonal to each other and that give rise to *nonzero* (dipole) amplitudes already in first order in the perturbation expansion of the photoionization amplitude [Eq. (1)], if the overlap of all the one-electron orbitals are treated properly. For a complete expansion of the initial and final states, such a "relaxation model" is quite equivalent to a second-order perturbation calculation (and even includes some contributions from higher orders), although the procedure and its sensitivity to deviations in the wave function representation differs. To calculate the relaxed-orbital photoionization amplitudes, we applied the recently extended components PHOTO of the RATIP program [24] in which the "nonorthogonality" of the electron orbitals is included by following Löwdin's expressions [25].

D. Auger amplitudes and rates

Apart from the photoionization of the ground state, the Auger amplitudes and rates are needed to understand the subsequent electron emission from inner-shell excited hole states. These amplitudes arise from the coupling of the hole states to the electron continuum due to the interaction among the bound-state electrons but is affected also by the configuration mixing between different autoionization channels in the course of the emission process, i.e., by the so-called interchannel interactions. However, apart from very few case studies on the K-LL and K-LM spectra of rare-gas atoms [26,27], it long has been common practice to neglect both the interchannel interactions as well as the nonorthogonality in the evaluation of the many-electron Auger amplitudes. The assumption of a common set of *orthonormal* orbitals for the intermediate hole state and final states of the ion means that the transition operator $H - E_m$, which contains the atomic Hamiltonian H and the total energy E_m of the intermediate hole state $|m\rangle$, can be replaced by the electron-electron interaction $H - E_m \approx V$. Moreover, for light and medium elements, it is typically sufficient to include the instantaneous Coulomb repulsion between the electrons, $V = \sum_{i<j} 1/|\vec{r}_i - \vec{r}_j|$, and to omit further relativistic contributions to the electron-electron interaction. Indeed, the restriction to the electron-electron interaction in the computation (many-electron) Auger amplitudes is standard in all Auger codes available at present, even if the orbital functions of the resonant state $|m\rangle$ and the final ionic state $|f\rangle$ are not fully orthogonal to each other due to the particular procedure with which the wave functions are generated. This computational scheme is realized also by the AUGER component of the RATIP program, in which the continuum spinors are solved within a spherical but level-dependent potential of the final ion (the so-called *optimal level* scheme in the GRASP92 program); this scheme also includes the exchange interaction of the emitted electron with the bound-state density. Again, a rather large number of scattering states $|\gamma_f J'_f P'_f, \epsilon\kappa_c : \gamma_t J_t P_t\rangle$ of a system occur quite frequently as the free electron may couple in quite different ways to the bound-state electrons. For further details on the computations of the Auger matrix elements and relative intensities, we refer the reader to Ref. [28].

Having a more or less simple access to the (double) photoionization and Auger amplitudes, we can simulate electron spectra for triple ionization of krypton, starting from its $^1S_0$ ground state. The energies and width of the individual hole states can be calculated with an accuracy which is usually sufficient for their *identification*, while the absolute energies and widths were better taken from previous measurements for a direct comparison of the peak intensities between experiment and theory.

IV. RESULTS

In order to illustrate the physical process investigated in the present work, Fig. 1 shows a schematic energy level diagram for various charge states of Kr, including several $3d^9 4p^5$ states of Kr^{2+} populated by primary double photoionization as well as several states of Kr^{3+} populated by secondary Auger decay. The kinetic energy of the Auger electron is determined by the energy difference between the intermediate $3d^9 4p^5$ state and the energy of the final Kr^{3+} state involved in the transition.

Figure 2 displays a map of three-electron coincidence events, recorded at the photon energy of 150 eV, with the sum of the kinetic energies of two electrons on the (y)

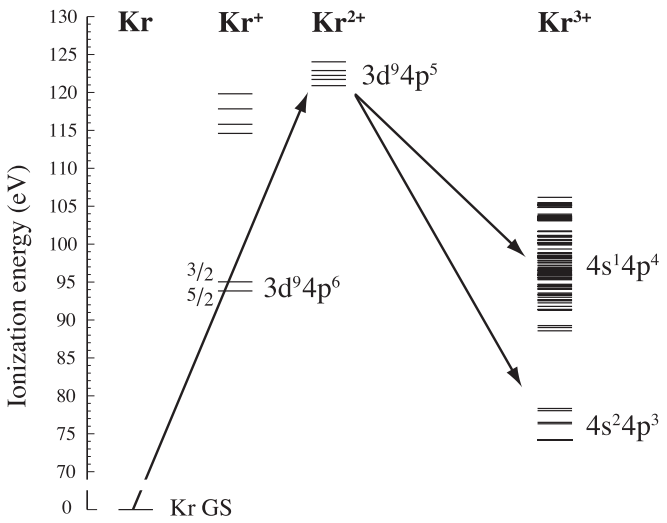

FIG. 1. Schematic energy level diagram of krypton in various charge states illustrating the processes studied in this work. Energy values given are based on data from Refs. [17,29–31]. The energy levels of Kr^{3+} taken from NIST [31] have been corrected by 1.2 eV (see text for details).

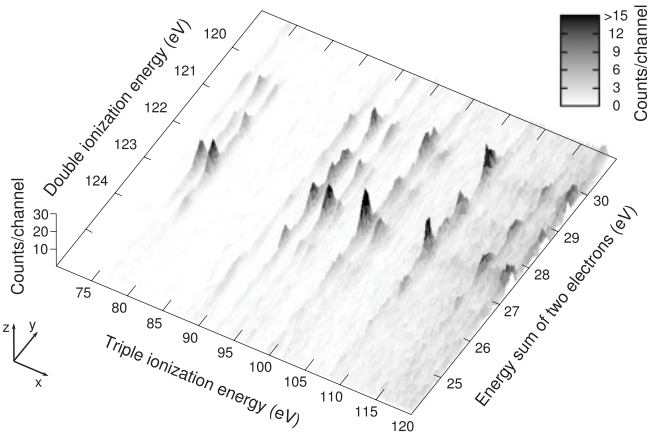

FIG. 2. Triple electron coincidence map recorded at the photon energy $h\nu = 150$ eV, which shows the formation of Kr^{3+}states by single Auger decay from Kr^{2+} $3d^9 4p^5$ intermediate states. The y axis represents the kinetic energy sum of two electrons (a projection of it is shown in Fig. 3) which reflects the core-valence intermediate states. The x axis represents the photon energy minus the total kinetic energy sum of all three electrons detected (the projection of it is shown in Fig. 4), and the z axis represents coincidence counts per channel.

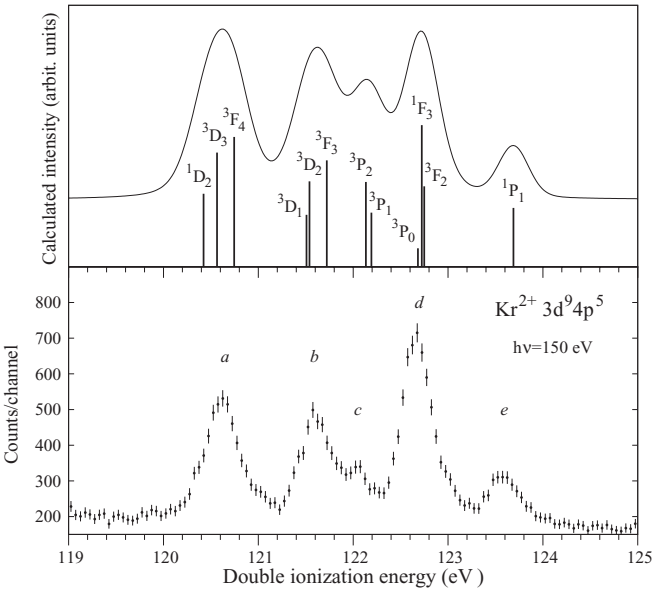

FIG. 3. Lower panel: Single photon core-valence double-ionization spectra of krypton recorded at $h\nu = 150$ eV, obtained by integration along the x axis of the data presented in Fig. 2. Upper panel: Simulated spectrum using the calculated Kr^{2+} $3d^9 4p^5$ state energies and photoionization amplitudes, convoluted with the expected experimental resolution and calculated lifetime widths. The calculated levels and relative intensities are indicated by bars, together with LS term symbols.

axis and the total kinetic energy sum of all three electrons emitted on the (x) axis. The map shows several distinct areas of enhanced intensity. Since the $3d^9 4p^5$ states have ionization energies between 120 and 125 eV [30,32,33], the two photoelectrons will share, at the present photon energy of $h\nu = 150$ eV, a kinetic energy sum in the range 25 to 30 eV while the subsequent Auger electron will lie in the energy range between 0 and 50 eV. Therefore, we cannot distinguish, with certainty, the photoelectrons from the Auger electron if the Auger electron has less than 30 eV kinetic energy or, referring to Fig. 2, for states of Kr^{3+} with ionization energies above 90 eV. However, in the present work we investigate the energy sum of two electrons and, therefore, the energy sum of *one* photoelectron and the Auger electron will not be constant, unless the energy distribution of the photoelectrons is structured. Hence, it will not result in any additional peak structures in Fig. 2 but will instead increase the background for that specific triple ionization energy. The contribution to the background due to this "false counting" can be estimated from the possible electron kinetic energies.

Along the x axis of Fig. 2 at triple ionization energies between 74 and 80 eV we see three lines of increased intensity (see also Fig. 4). These peaks correspond to the $^4S_{3/2}$, $^2D_{5/2,\,3/2}$, and $^2P_{3/2,\,1/2}$ states of the $4s^2 4p^3$ configuration, which were examined in some detail before [12]. The relative intensities of these three lines differ from the ones presented in Ref. [12], since in the present study we focus on a specific triple ionization mechanism in contrast to the work of Ref. [12] where several mechanisms contributed to the final state spectrum of the trication.

Along the y axis of Fig. 2, we see a group of peaks at double-ionization energies between 120 and 125 eV. These features were labeled "group II" in Ref. [12], and we will examine them in more detail in the present work. As established in Ref. [12] and as we will elaborate on in what follows, this group of features is associated with a direct double-photoionization process. Indeed, the kinetic energy sum of two electrons at the photon energy chosen agrees well with the energies of the $3d^{-1}\,4p^{-1}$ core-valence states of doubly ionized krypton, as previously found by Bolognesi *et al.* [30].

In the lower panel of Fig. 3 we show the Kr^{2+} $3d^9 4p^5$ spectrum where five peak structures, labeled a to e, are discernible. Their peak positions and areas are listed in Table I. The experimental spectrum is quite similar to the one recorded near threshold by Bolognesi *et al.* [30] as shown in Fig. 1 of this reference. As previous works [30,32–34] and the calculations in the present work indicate, only peak e is expected to correspond to a single state, assuming the instrumental resolution in the present work. A reliable deconvolution of peaks a to d into peaks corresponding to individual states proved difficult for the present data set, due to the lack of counting statistics and precise knowledge

TABLE I. Experimental energy values and intensities related to the $3d^9 4p^5$ core-valence states. Error estimates of energies are given by the last digit, unless otherwise stated. Uncertainty in the energy calibration of the energy region corresponding to the core-valence states introduces an additional error of ±50 meV to the energy scale.

Label	Assignment	Peak center (eV)	Peak area (arb. units)
a	($^1D_2$, $^3D_3$, $^3F_4$)	120.6	73
b	($^3D_1$, $^3D_2$, $^3F_3$)	121.6	55
c	($^3P_2$, $^3P_1$)	122.0	14
d	($^3P_0$, $^1F_3$, $^3F_2$)	122.7	100
e	$^1P_1$	123.59 ± 0.02	25

of the spectral line profile, which is needed when fitting unresolved features. The peak positions and areas listed in Table I were extracted from a fit to five Gaussian functions and a baseline represented by a polynomial function, which we expect to be a good approximation for the $^1P_1$ state (peak *e* in Fig. 3) and a reasonable estimate of the peak centroids of the partially resolved peaks *a* to *d* in Fig. 3. We note that the ionization energy for the $^1P_1$ state obtained in the present work is in very good agreement with previous $M_{4,5}N_{2,3}$-*NNN* Auger measurements [32–34], if the lowest triple ionization energy of Kr^{3+} is assumed to be 74.197 eV, as reported by Palaudoux *et al*. [13].

The kinetic energy distribution of the two photoelectrons does not reveal any marked structures in the present data but is, instead, quite flat, which suggests a direct core-valence double-ionization mechanism for the primary process. The only exception we find is the double-ionization energy region corresponding to peak *a* in Fig. 3 and, in this case, preferentially when an Auger decay to the triply ionized ground state occurs in succession. In investigating the decays to the first few excited triply ionized states, we find that the structures in the kinetic energy distributions gradually disappear with increasing triple ionization energy. Such a tendency seems to be inconsistent with formation and decay of a core-valence ionized state and we conclude that the structured energy distribution does not arise from core-valence double ionization. A possible origin of the artifact is $4d^{-1}4p^{-1}nl$ singly ionized states with ionization energies (see Ref. [30]) close to that of the core-valence doubly ionized states. These singly ionized states can decay to low-lying triply ionized states via an Auger cascade, in which case it is likely that one Auger electron has low kinetic energy and the other high. The energy sum of the photoelectron, which in this case has a fixed energy, and a low-energy Auger electron would then partly overlap with the core-valence states. We believe the area of enhanced intensity seen in Fig. 2 extending toward double-ionization energies (*y* axis) below 120 eV and which appears in connection with decay to the triply ionized ground state has a similar origin.

In the upper panel of Fig. 3 a simulated core-valence spectrum is shown. The spectrum was constructed using 12 energy levels and the corresponding photoionization amplitudes, which were calculated based on the multiconfigurational approach described in the previous section, and convoluted with the experimental resolution and calculated lifetimes of the states. The energies and relative intensities used are indicated below the spectrum by bars. As can be seen, the agreement of the simulated spectrum compared to the experimental one shown in the lower panel of Fig. 3 is good, with the exception of the $^3P_0$, $^1F_3$, and $^3F_2$ states, whose intensity appear to be underestimated in the calculations. The calculated energies, intensities, and the corresponding *LS* terms are listed in Table II. Our assignment is consistent with Ref. [33] and with Ref. [32] for the transitions which were possible to assign in those works. Discrepancies from some of the assignments given in Ref. [30] are noted. In the present work the calculated energy levels have been shifted by 2.85 eV in order to adjust the lowest three states to the experimental peak *a*.

The $3d^94p^5$ states can decay to a fairly large number of Kr^{3+} states by single Auger transitions. The resulting spectrum is presented in Fig. 4(a), where several structures, labeled 1 to 12, are visible. Their energies and the areas of the peaks are given in Table III. The first seven peak structures can be assigned with the aid of the NIST database [31], which is done in the upper part of the spectrum where leading configurations and *LS* term symbols are given. Since several recent studies (see, e.g., Ref. [7] and references therein) found that the Kr^{3+} $4s^24p^3\ ^4S_{3/2}$ ground state is approximately 1 eV below the value listed in NIST, this correction has been taken into account for all energy levels which were plotted based on NIST in Fig. 4(a).

TABLE II. Calculated $3d^94p^5$ energy levels and photoionization cross sections, normalized to 100. The levels are related to the lowest-lying $^1D_2$ state.

Energy (eV)	Intensity (arb. unit)	*LS* term
0	52	$^1D_2$
0.14	81	$^3D_3$
0.32	92	$^3F_4$
1.09	37	$^3D_1$
1.12	60	$^3D_2$
1.30	75	$^3F_3$
1.71	60	$^3P_2$
1.77	38	$^3P_1$
2.26	13	$^3P_0$
2.30	100	$^1F_3$
2.30	57	$^3F_2$
3.27	42	$^1P_1$

To gain a deeper understanding of the ionization processes, we have performed extensive calculations for the energy levels of Kr^{3+} and Auger rates for transitions from the 12 intermediate $3d^94p^5$ states to various Kr^{3+} final states studied

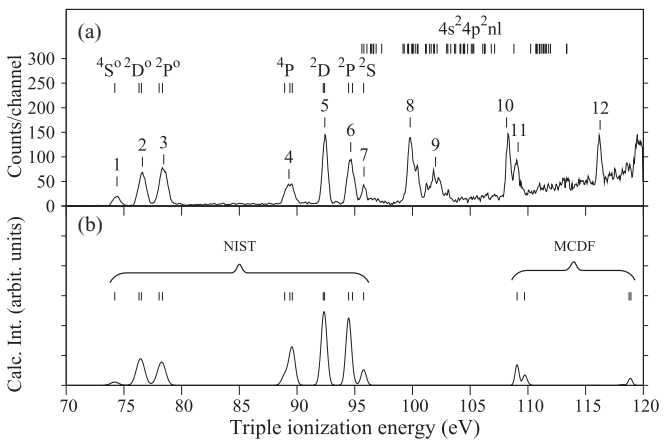

FIG. 4. (a) Kr^{3+} electron spectrum formed by single Auger decay from Kr^{2+} $3d^94p^5$ intermediate states, obtained by integration along the *y* axis of the data presented in Fig. 2. Energy levels from the NIST database [31] are indicated by bars. (b) A simulated spectrum based on calculated energy levels and Auger rates (see text), convoluted with the experimental resolution. Some of the calculated level energies have been replaced by experimental ones from the NIST database, as explained in the text, which is indicated in the spectrum. Auger rates have been weighted by intensities from Table II corresponding to the intermediate state involved in the transition.

TABLE III. Experimental Kr^{3+} lines and calculated transition rates normalized to peak 5 in Fig. 4. The uncertainty in the absolute energy of the lowest-lying peak 1 is estimated to be 150 meV. The error in relative energies are a function of the energy separation and increase from 20 meV for close-lying peaks (0–5 eV) to 100 meV for a separation of 40 eV. The calculated intensity have been obtained by summing the Auger rates from all the initial Kr^{2+} states of Table II to the calculated Kr^{3+} states, weighted by the calculated cross section of the initial state, as given in Table II. When several calculated Kr^{3+} states are associated with one experimental peak (see Fig. 6), the corresponding Auger rates have been added.

Label	Energy (eV)	Assignment		Peak area (arb. unit)	Calculated intensity (arb. unit)
1	74.35	$4s^24p^3$	$^4S^o$	20	60
2	76.59		$^2D^o$	71	50
3	78.41		$^2P^o$	90	44
4	89.35	$4s^14p^4$	^4P	50	70
5	92.41		^2D	100	100
6	94.64		^2P	74	88
7	95.78		^2S	12	19
8	100.0			117	
9	102.0			83	
10	108.3	$4s^04p^5$		64	19
11	109.0			34	10
12	116.2			32	

here. Using the calculated Auger rates from the Kr^{2+} $3d^94p^5$ intermediate states, we have constructed a theoretical triple ionization spectrum, which is shown in Fig. 4(b). When constructing the spectrum we have normalized the total Auger rate from each $3d^94p^5$ state to 1 and weighted each Auger transition by the calculated photoionization cross section of the intermediate $3d^94p^5$ state in question. The Kr^{3+} level calculations were made using the $4s^24p^3$, $4s^14p^4$, and $4s^04p^5$ configurations for the description of the Kr^{3+} final-state wave function, where we included single excitations to the $5s$, $5p$, and $5d$ subshells. It was recognized earlier that the Kr^{3+} levels are strongly affected by configuration interaction [35]. In particular, the levels in the triple ionization energy region 85 to 97 eV, where the experimental spectrum in Fig. 4(a) reveals four strong peaks, has been shown to be influenced by the $4s^14p^4 \Leftrightarrow 4s^24p^24d$ configuration interaction [35]. In order to account for this in the present Auger calculations, it would be necessary to also include double excitations from the $4s$ and $4p$ subshells, which proved not to be feasible within the current computational framework due to the large number of states. Because of the restricted computational model used, some of the MCDF energies are shifted by several eV and for the simulated spectrum in Fig. 4(b) we have, therefore, used the MCDF levels for identification of the transition but, whenever possible, used energies taken from optical spectroscopy, as given in the NIST tables. In this way we have used experimentally determined energies for the Auger transitions to the first 12 calculated states, which is also indicated in Fig. 4(b). We note that in the calculations transitions to these 12 states are the cause of all the intensity below the 97-eV triple ionization energy in Fig. 4(b).

Despite our restrictions in the expansion of the wave functions, the MCDF calculations reproduce the experimental spectrum rather well. The clearest discrepancy is the absence of any structure between 97- and 105-eV triple ionization energy in the calculations, whereas the experiment reveals two intense peaks, labeled 8 and 9 in Fig. 4(a), which both appear to have substructure. An extended calculation was carried out where specific double excitations were allowed in order to include the $4s^24p^24d$ and $4s^24p^25s$ configurations for the approximation of the final-state wave function. Although these calculations gave rise to intensity in the triple ionization energy region between 97 and 105 eV, they suffered from stability problems and led to Auger rates that varied in a rather unsystematic manner. However, these computations clearly showed that many levels of Kr^{3+} contribute to peaks 8 and 9 in Fig. 4(a) but that both an improved experimental resolution as well as much more elaborate computations will be needed for a detailed assignment in this triple ionization energy region. At ionization energies around 108 eV in Fig. 4(a), a strong doublet peak structure (peaks 10 and 11) is seen in the experimental spectrum. A similar feature is also present in the calculated spectrum, although shifted in energy by approximately 1 eV. The calculations show that two levels of Kr^{3+} are involved in this transition, with leading configuration $4s^04p^5$.

A strength of electron coincidence data is that various boundary conditions on the data can be applied which allows for more detailed investigation of ionization processes, for instance, requiring that the energies of one or several electrons

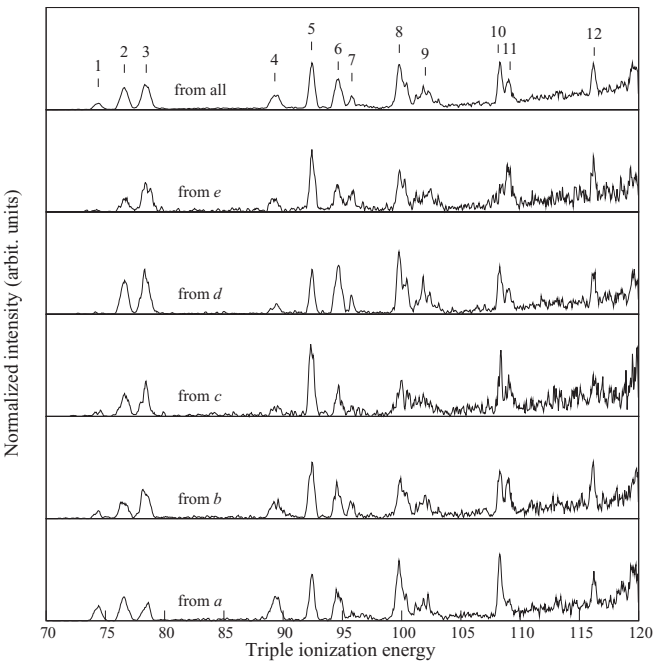

FIG. 5. Triple ionization spectra selected on the different core-valence intermediate state energy regions labeled *a*–*e* in Fig. 3. The triple ionization spectrum for decays from the entire spectral region of Fig. 3 is shown in the topmost panel in this figure. The intensities have been normalized with respect to the total intensity in the region between 70- and 110-eV ionization energy; the region above 110-eV energy has been excluded due to increased background noise.

lie within in a certain interval. From Fig. 2 it is clear that the decay paths from the intermediate $3d^9 4p^5$ states vary to a considerable extent. By selecting different portions of the map we can investigate these differing decay routes in further detail. In Fig. 5, we show electron spectra of the trication selected according to the peak structures *a*–*e* of Fig. 3. The top panel displayed in this figure shows the spectrum summed over the entire $3d^9 4p^5$ region (see also Fig. 4). Some of these decays have been studied earlier by normal Auger spectroscopy (see, e.g., Kivimäki *et al.* [34]). However, with the noncoincidence method used in Ref. [34], it is often difficult to reveal detailed information on congested electronic states, giving rise to overlapping spectral features.

In comparison to Fig. 5, the calculated Auger rates from each individual $3d^9 4p^5$ intermediate state are shown in Fig. 6. The total Auger rate from each intermediate $3d^9 4p^5$ state has been normalized to 1. The 12 calculated spectra of are grouped according to the experimental peak structures *a*–*e* of Fig. 3. On the left-hand side of the figure, *LS* term symbols are given to identify the intermediate states involved.

In Fig. 5, it can be seen that Auger decay to the ^4S triply charged ground state occurs predominantly from the core-valence intermediate states associated with peak structure

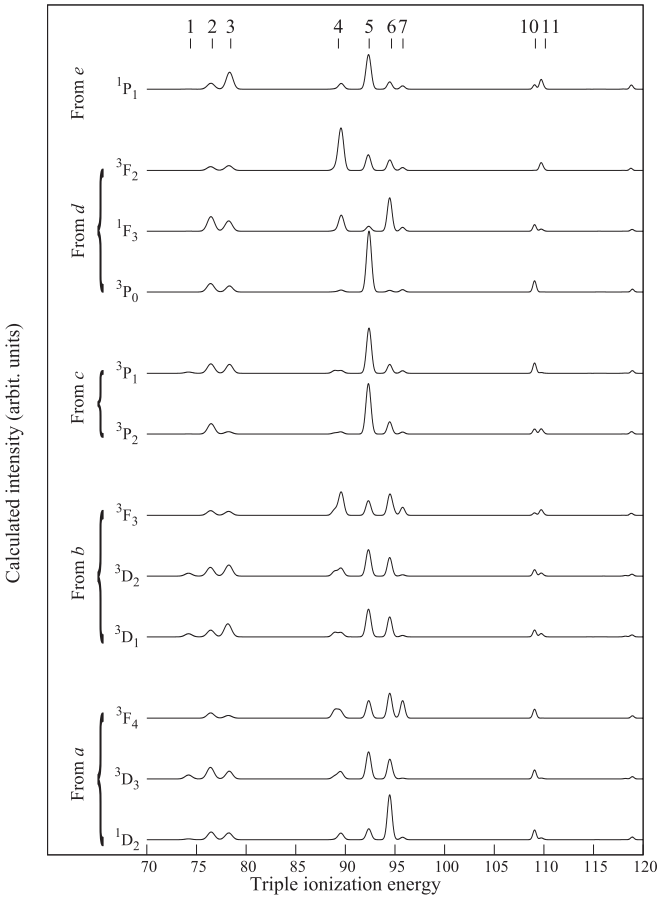

FIG. 6. Simulated Auger-electron spectrum for transitions from Kr^{2+} $3d^9 4p^5$ states to Kr^{3+}, based on calculated Auger rates. The *LS* terms for the individual intermediate states are given together with the label (*a* to *e*) of the corresponding experimental Kr^{2+} $3d^9 4p^5$ peak (cf. Fig. 3). At the top of the graph the label of the corresponding experimental peak is given (cf. Figs. 4 and 5).

a, and to a lesser degree also from peak structure *b* of Fig. 3. Indeed, the calculations presented in Fig. 6 confirm this finding and identify a $^3D_3$ core-valence state to be responsible for the contributions of peak *a*, as well as $^3D_1$ and $^3D_2$ core-valence states to be responsible for the contributions of peak *b*. Interestingly, all core-valence states contributing to the formation of the ^4S trication state are ^3D states.

In the topmost spectrum of Fig. 5 peak 2 (^2D) is about 5 times stronger than peak 1 (^4S). According to the selected triple-ionization spectra shown in this figure, all intermediate core-valence states associated with peaks *a* to *e* of Fig. 3 contribute to the population of these final tricationic states. Apparently, the decay to the ^2D states occurs with similar probability from intermediate states associated with peak structures *a* to *c*, while the decay from intermediate states associated with peak structure *d* and *e*, respectively, is about twice and half as probable, respectively. Interestingly, according to the calculations, the Auger rate associated with transitions from peak structure *d* has a strong contribution from the $^1F_3$ intermediate state, while the $^1P_1$ intermediate state belonging to peak structure *e* does not seem to contribute much to the formation of the ^2D tricationic states. Both findings fit qualitatively well to the experimental observations.

Peak 3 (^2P) in the topmost spectrum of Fig. 5 is only slightly more intense than peak 2 (^2D) in this spectrum, and, again, all intermediate $3d^9 4p^5$ states contribute to the Auger decays. In comparison to the decays to the ^2D states, the probability for decay to the ^2P states as a function of the intermediate state varies in a quite similar fashion for the intermediates states associated to peaks *a* to *d* in Fig. 3. The decay from the intermediate state $^1P_0$ associated with peak *e* in Fig. 3 is, however, more than twice as likely to lead to ^2P states than to ^2D states of Kr^{3+}.

In looking at the excited tricationic states observed at ionization energies above 87 eV, peak 5 (^2D) is prominent in both the experimental and theoretical data. Apparently, it is very strong in all the experimental Auger spectra presented in Fig. 5, and it is populated by the decays from all the intermediate state region *a* to *e* in Fig. 3. The latter is confirmed by our calculations which suggest that the ^3P intermediate states give significant contribution to the Auger transitions in this spectral region.

The intensity of peak 4 (^4P) varies quite a bit as a function of the intermediate core-valence states as seen from the spectra shown in Fig. 5. Akin to the population of the outermost tricationic state (peak 1), most of the intensity seems to originate from decays involving intermediate states associated with peaks *a* and *b* from Fig. 3.

The interpretation of the Auger rates for transitions to the more highly excited tricationic states gets gradually more difficult, since most likely several electronic configurations, of which some may have been neglected in the present calculations, mix strongly in this spectral region. The neglect of some electron configurations may already explain several of the discrepancies noted for the lower Kr^{3+} states.

V. CONCLUSIONS

The core-valence double-photoionization spectrum of Kr associated with the $3d^9 4p^5$ configuration has been recorded

and shows four distinct features in the ionization energy range between 120 and 125 eV. Assignment of these structures have been made based on MCDF calculations. The subsequent Auger decay into triply charged final states primarily connected to the $4s^2 4p^3$ and $4s^1 4p^4$ configurations was also recorded in coincidence with the photoelectrons. A number of spectral features were observed between 70- and 120-eV ionization energy and were assigned with the help of MCDF calculations of energies and Auger rates. A detailed comparison between the experimental and numerical results was made and showed that the decay channels are highly selective. In particular, strong transitions are observed from triplet states of Kr^{2+}.

ACKNOWLEDGMENTS

The authors thank Dr. S. Butorin for preliminary calculations and fruitful discussions. This work has been financially supported by the Swedish Research Council (VR), the Göran Gustafsson Foundation (UU/KTH), the Knut and Alice Wallenberg Foundation, and the Wenner-Gren Foundations, Sweden. S.F. acknowledges the support by the FiDiPro programme of the Finnish Academy. This work was also supported by the European Community–Research Infrastructure Action under the FP6 "Structuring the European Research Area" Programme (through the Integrated Infrastructure Initiative "Integrating Activity on Synchrotron and Free Electron Laser Science," Contract No. R II 3-CT-2004-506008).

[1] K. Siegbahn, C. Nordling, G. Johansson, J. Hedman, P. Hedén, K. Hamrin, U. Gelius, T. Bergmark, L. O. Werme, R. Manne, and Y. Baer, *ESCA Applied to Free Molecules* (North-Holland, Amsterdam 1969).

[2] J. Eland, *Photoelectron Spectroscopy* (Butterworths, London, 1974).

[3] T. Carlson, *Photoelectron and Auger Spectroscopy* (Plenum, New York, 1975).

[4] P. Kruit and F. H. Read, J. Phys. E **16**, 313 (1983).

[5] J. H. D. Eland, O. Vieuxmaire, T. Kinugawa, P. Lablanquie, R. I. Hall, and F. Penent, Phys. Rev. Lett. **90**, 053003 (2003).

[6] Y. Hikosaka, P. Lablanquie, F. Penent, T. Kaneyasu, E. Shigemasa, R. Feifel, J. H. D. Eland, and K. Ito, Phys. Rev. Lett. **102**, 013002 (2009).

[7] J. H. D. Eland, P. Linusson, L. Hedin, E. Andersson, J.-E. Rubensson, and R. Feifel, Phys. Rev. A **78**, 063423 (2008).

[8] F. Penent, J. Palaudoux, P. Lablanquie, L. Andric, R. Feifel, and J. H. D. Eland, Phys. Rev. Lett. **95**, 083002 (2005).

[9] J. Viefhaus, M. Braune, S. Korica, A. Reinköster, D. Rolles, and U. Becker, J. Phys. B **38**, 3885 (2005).

[10] P. Lablanquie, L. Andric, J. Palaudoux, U. Becker, M. Braune, J. Viefhaus, J. Eland, and F. Penent, J. Electron Spectrosc. Relat. Phenom. **156–158**, 51 (2007).

[11] J. Palaudoux, P. Lablanquie, L. Andric, J. H. D. Eland, and F. Penent, J. Phys.: Conf. Ser. **141**, 012012 (2008).

[12] E. Andersson, S. Fritzsche, P. Linusson, L. Hedin, J. H. D. Eland, J.-E. Rubensson, L. Karlsson, and R. Feifel, Phys. Rev. A **82**, 043418 (2010).

[13] J. Palaudoux, P. Lablanquie, L. Andric, K. Ito, E. Shigemasa, J. H. D. Eland, V. Jonauskas, S. Kučas, R. Karazija, and F. Penent, Phys. Rev. A **82**, 043419 (2010).

[14] K. Sawhney, F. Senf, M. Scheer, F. Schäfers, J. Bahrdt, A. Gaupp, and W. Gudat, Nucl. Instrum. Methods A **390**, 395 (1997).

[15] E. Andersson, M. Stenrup, J. H. D. Eland, L. Hedin, M. Berglund, L. Karlsson, A. Larson, H. Ågren, J.-E. Rubensson, and R. Feifel, Phys. Rev. A **78**, 023409 (2008).

[16] [http://www.bessy.de].

[17] G. C. King, M. Tronc, F. H. Read, and R. C. Bradford, J. Phys. B **10**, 2479 (1977).

[18] L. O. Werme, T. Bergmark, and K. Siegbahn, Phys. Scr. **6**, 141 (1972).

[19] I. P. Grant, *Methods in Computational Chemistry*, edited by S. Wilson (Plenum Press, New York, 1988).

[20] S. Fritzsche, A. Surzhykov, and T. Stöhlker, Phys. Rev. A **72**, 012704 (2005).

[21] N. Kabachnik, S. Fritzsche, A. Grum-Grzhimailo, M. Meyer, and K. Ueda, Phys. Rep. **451**, 155 (2007).

[22] S. Fritzsche, Phys. Scr. **2002**, 37 (2002).

[23] F. A. Parpia, C. Froese Fischer, and I. P. Grant, Comput. Phys. Commun. **94**, 249 (1996).

[24] S. Fritzsche, J. Electron Spectrosc. Relat. Phenom. **114–116**, 1155 (2001).

[25] P.-O. Löwdin, Phys. Rev. **97**, 1474 (1955).

[26] S. Fritzsche, B. Fricke, and W.-D. Sepp, Phys. Rev. A **45**, 1465 (1992).

[27] J. Tulkki, N. M. Kabachnik, and H. Aksela, Phys. Rev. A **48**, 1277 (1993).

[28] S. Fritzsche, Phys. Lett. A **180**, 262 (1993).

[29] B. Eriksson, S. Svensson, N. Mårtensson, and U. Gelius, J. Phys. Colloques **48**, 531 (1987).

[30] P. Bolognesi, L. Avaldi, M. C. A. Lopes, G. Dawber, G. C. King, M. A. MacDonald, C. Villani, and F. Tarantelli, Phys. Rev. A **64**, 012701 (2001).

[31] Y. Ralchenko, A. Kramida, J. Reader, and NIST ASD Team (2010), *NIST Atomic Spectra Database* (ver. 4.0.1), [Online]. Available: [http://physics.nist.gov/asd] [2011, December 16] (National Institute of Standards and Technology, Gaithersburg, MD).

[32] L. Partanen, M. Huttula, H. Aksela, and S. Aksela, J. Phys. B **40**, 3795 (2007).

[33] J. Jauhiainen, A. Kivimaki, S. Aksela, O. P. Sairanen, and H. Aksela, J. Phys. B **28**, 4091 (1995).

[34] A. Kivimäki, H. Aksela, J. Jauhiainen, A. Naves de Brito, O.-P. Sairanen, S. Aksela, A. Ausmees, S. J. Osborne, and S. Svensson, Phys. Rev. A **49**, 5124 (1994).

[35] W. Persson and S.-G. Pettersson, Phys. Scr. **29**, 308 (1984).